Multiple Organic Carbon Isotope Reversals across the Permo-Triassic Boundary of Terrestrial Gondwana Sequences: Clues to Extinction Patterns and Delayed Ecosystem Recovery

Maarten J. de Wit, Joy G. Ghosh,[1] *Stephanie de Villiers,*[2] *Nicolas Rakotosolofo,*[3] *James Alexander, Archana Tripathi,*[4] *and Cindy Looy*[5]

Centre for Interactive Graphical Computing of Earth Systems (CIGCES), Geological Sciences, University of Cape Town, Rondebosch 7701, South Africa
(*e-mail: maarten@cigces.uct.ac.za*)

ABSTRACT

Organic materials across the palynologically defined Permian-Triassic (P-T) boundary from five major terrestrial basins in the interior of the former Gondwana Supercontinent show large to very large (5‰–15‰) multiple negative spikes of $\delta^{13}C$, separated in places by sharp reversals of up to 20‰. Large oscillations of $\delta^{13}C_{org}$ between −36‰ and −15‰ from mean values of ~24 ± 2 in India, ~26 ± 2 in Madagascar, and ~23 ± 2 in South Africa occur before and after the P-T transition. The mean values are within the range of modern C3 plants (~−25‰). The negative $\delta^{13}C_{org}$ spikes of the terrestrial plant remains complement similar spikes of smaller amplitude recorded globally in marine carbonates across the P-T boundary. Sensitivity analyses of carbon fluxes in a coupled atmosphere-ocean system indicate that the sharp declines in terrestrial and marine $\delta^{13}C$ can be explained by episodic release of methane from clathrates (~−60‰) either directly into the atmosphere or via the oceans, possibly during the disintegration of the southern continental shelf of Tethys. The rapid increases in $\delta^{13}C$ may either signal aborted attempts of C4 plants (~−13‰) to establish themselves at the expense of C3 plants or, more likely, reflect a punctuated increase in C3 biomass production related to elevated atmospheric CO_2. Detection of a gradual negative trend in the Upper Permian and a similar positive recovery in the Lower Triassic, separated by up to three large negative $\delta^{13}C$ spikes across the P-T boundary in at least four terrestrial sections, caution against models of the end-Paleozoic biodiversity collapse and ensuing Mesozoic recovery based on a singular perturbation at the P-T boundary. Rather, these transitions may reflect multiple ecosystem stability states and abrupt responses during gradual forcing of a complex nonlinear system with thresholds.

Introduction

Stratigraphic transitions from the Permian to the Triassic around 251 Ma (Menning 2001) record extensive global collapse and recovery of biodiversity. Extinctions in marine and terrestrial life across the boundary were abrupt, at >90% and 70% species level, respectively (Erwin 1993, 1994; Retallack 1995, 1999; Hallam and Wignall 1997; Jin et al. 2000). Yet there is circumstantial evidence that environmental stresses on ecosystems preceded this global crisis by at least several million years (Baud et al. 1989; Thackeray et al. 1990; Margaritz et al. 1992; Stanley and Yang 1994; Faure et al. 1995; Retallack 1995; Knoll et al. 1996) and substantial evidence that, in the wake of the extinction, maximum biosphere recovery was delayed until at least the Middle Triassic (~245 Ma; Eshet et al. 1995; Retallack 1995; Visscher et al. 1996; Looy et al. 1999; Erwin 2000). Such observations suggest a sustained and complex feedback mechanism during the buildup and dissipation of this global ecological crisis (Erwin 1993; Faure et al. 1995; Knoll et al.

Manuscript received December 2, 2000; accepted August 19, 2001.

[1] Current address: Geological Survey of India, Geochronology and Isotope Geology Division, 15 Kyd Street, Calcutta 7000-16, India.

[2] Current address: Department of Earth Sciences, Downing Street, University of Cambridge, Cambridge CB2 3EQ, United Kingdom.

[3] Current address: Institute for Geophysics, Ludwig-Maximillians University, Munich 80333, Germany.

[4] Birbal Sahni Institute of Palaeobotany, 53 University Road, Lucknow 226007, India.

[5] Laboratory of Palaeobotany and Palynology, Utrecht University, Budapestlaan 4, 3584 CD, Utrecht, The Netherlands.

[The Journal of Geology, 2002, volume 110, p. 227–240] © 2002 by The University of Chicago. All rights reserved. 0022-1376/2002/11002-0007$15.00

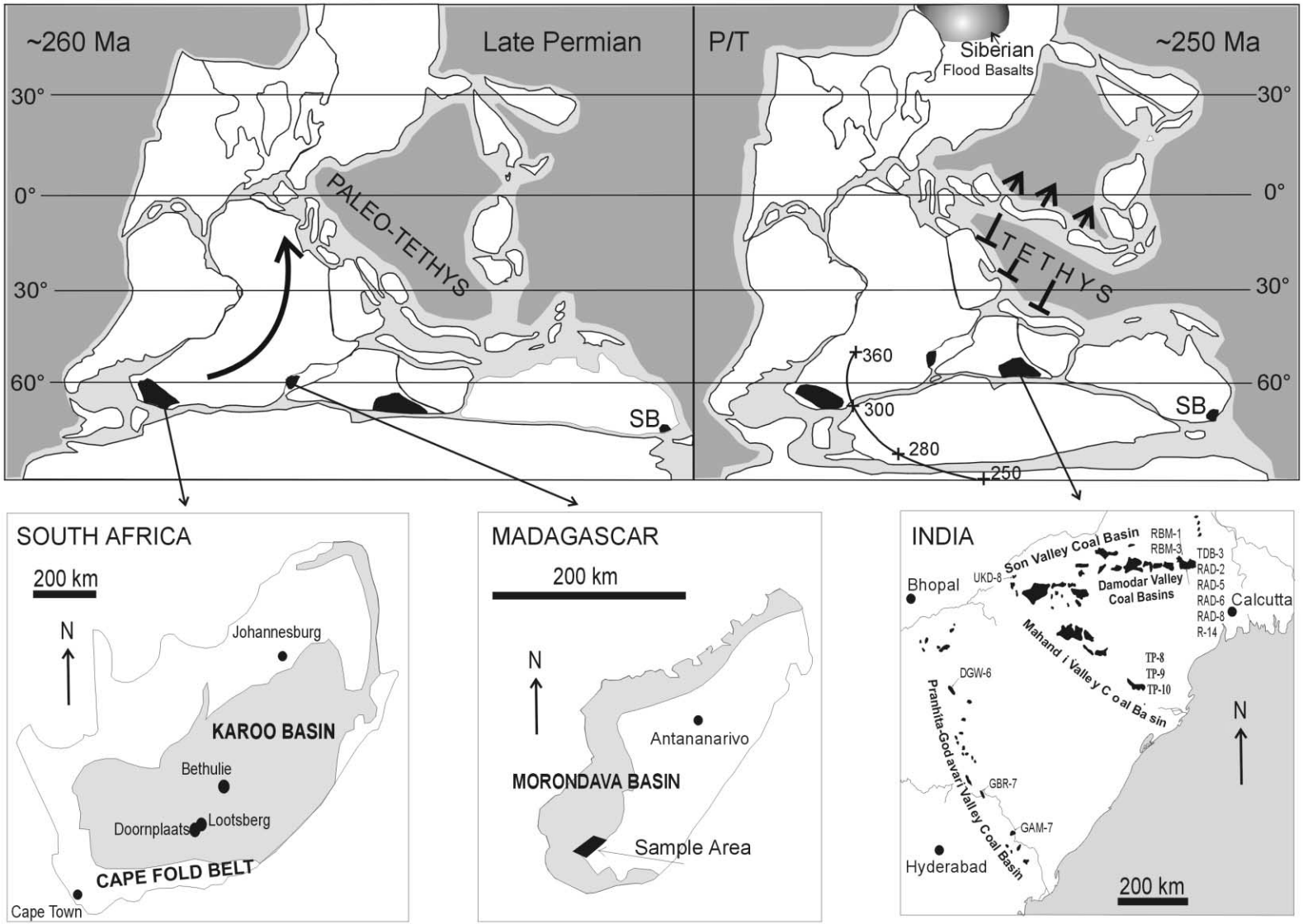
~260 Ma
Late Permian
P/T
~250 Ma
Siberian
Flood Basalts
30°
0°
30°
60°
PALEO-TETHYS
TETHYS
360
300
280
250
SB
SB
SOUTH AFRICA
200 km
N
Johannesburg
KAROO BASIN
Bethulie
Doornplaats
Lootsberg
CAPE FOLD BELT
Cape Town
MADAGASCAR
200 km
N
Antananarivo
MORONDAVA BASIN
Sample Area
INDIA
Bhopal
UKD-8
Son Valley Coal Basin
RBM-1
RBM-3
Damodar Valley
Coal Basins
TDB-3
RAD-2
RAD-5
RAD-6
RAD-8
R-14
Calcutta
Mahand i Valley C oal Ba sin
TP-8
TP-9
TP-10
DGW-6
Pranhita-Godavari Valley Coal Basin
GBR-7
GAM-7
Hyderabad
N
200 km

1996; Hallam and Wignall 1997) rather than a sudden reaction to an abrupt single event such as the rapid outpourings of the Siberian flood basalts or a cometary impact (Renne et al. 1995; Kamo et al. 1996; Bowring et al. 1998; Jin et al. 2000; Becker et al. 2001). It is important to be able to resolve different paleoecodynamic forces so that resulting patterns of biotic recovery and origination following extinction events can be analyzed and simulated with confidence.

Remarkable excursions in the $^{13}C/^{12}C$ ratios (expressed as $\delta^{13}C$) of both marine and terrestrial carbonates and organic matter across the P-T boundary reflect significant changes in the global carbon cycle. These studies have identified a large and sharp negative $\delta^{13}C$ spike that straddles the P-T boundary in marine sequences (Baud et al. 1989; Margaritz et al. 1992; Xu and Yan 1993; Yin et al. 1996; Krull et al. 2000; Twitchett et al. 2001). High-precision radiometric analysis of volcanogenic zircons in tuffs across the P-T boundary has dated the approximate peak of a negative excursion in a marine sequence of a northern Gondwana fragment (now southern China) at 251.4 ± 0.3 Ma (Bowring et al. 1998). This peak (confined to unit 27a) is closely linked with the major P-T extinction peak (Yin et al. 1996; Bowring et al. 1998; Jin et al. 2000). Because biostratigraphic correlations between marine and terrestrial sequences are notoriously difficult, one strategy has been to identify this $\delta^{13}C$ spike also across the P-T boundary in terrestrial environments and, in turn, as a marker for stratigraphic correlation and paleogeographic reconstructions (Morante 1996; MacLeod et al. 2000). However, the precise relationship between the biostratigraphy and chemical markers is not clear. In numerous marine sections along the southern platform margin of the paleo-Tethys ocean, a number of complex spikes have been recorded (Baud et al. 1989; Margaritz et al. 1992; Erwin 1993; Hallam and Wignall 1997). In some sections a peak minimum occurs in the Lower Triassic, yet elsewhere along the same Tethyan margin a minimum occurs in the Upper Permian (Baud et al. 1989; Margaritz et al. 1992; Morante 1996). Similarly, multiple peaks in the lowermost Triassic have been recorded from Jameson Land in Greenland (Oberhänsli et al. 1989). Moreover, these relatively rapid excursions are often superimposed on a gradual Upper Permian decline in $\delta^{13}C$, documented in both terrestrial and marine environments (Baud et al. 1989; Oberhänsli et al. 1989; Thackeray et al. 1990; Margaritz et al. 1992; Faure et al. 1995). In the marine sections of China, a second large negative $\delta^{13}C$ excursion and/or a series of more subdued negative pulses are also evident just above and below the main P-T boundary spike (Bowring et al. 1998; Metcalfe et al. 1999; Jin et al. 2000).

The major negative $\delta^{13}C$ spike in the marine section of China appears to be in response to a catastrophic addition of light carbon to the oceans in less than 170,000 yr (Bowring et al. 1998). There is, however, dispute about the cause of the negative excursion(s) (Erwin 1993; Faure et al. 1995; Renne et al. 1995; Kamo et al. 1996; Knoll et al. 1996; Morante 1996; Hallam and Wignall 1997; Bowring et al. 1998; Forster et al. 1999; Krull et al. 2000; MacLeod 2000; Twitchett 2000; Becker et al. 2001),

Figure 1. Changing position of Gondwana (in a Pangean framework) from about 260 (~end Guadalupian, Middle Permian) to 250 Ma (~Permian-Triassic boundary), modified from Scotese (2000) and Smith (1999). Gondwana basins of South Africa, Madagascar, and India discussed in this article are marked in black. Insets show details of samples. The NE continental margin of Gondwana shifted from dominantly midlatitudes (20°–60°S) to low latitudes (0°–40°S) during this time, while the basins remained at similar latitudes (60° ± 10°S). The Indian basins moved farthest, from ~70°S to ~50°S, due to the relative rotational displacement of Gondwana. By 245 Ma (end Induan), India progressed to ~40°S; simultaneously, the NE margin of Gondwana disintegrated into smaller continental fragments that dispersed (*arrows*) to later collide with Asia. This ~15-m.yr. period coincides with the onset and decline of widespread anoxia in the global deep oceans and includes a sharp climax of superanoxia across the P-T boundary that affected the shallow oceans as well (Isozaki 1997). This period also overlaps with declining sea level to a eustatic lowstand at or just prior to ~250 Ma, followed by rapid sea level increase possibly related to combined effects of increase in spreading ridge length and subsidence of the stretched and rifted Tethyan fragments. Rifting and drifting processes, general warming, and changing modes of ocean dynamics may have catalyzed and sustained increased CH_4 flux into the ocean and atmosphere by destabilizing clathrate (CH_4 hydrate) deposits. Significant release of CO_2 into the atmosphere via the Siberian flood basalts started around ~251 Ma, while oxidation of coal deposits occurred during the global coal hiatus ~255–240 Ma (Faure et al. 1995; Retallack et al. 1996). Clearly, the global atmosphere-ocean system was stressed to a significant degree over at least 10–20 m.yr. Crosses indicate the location of paleomagnetic south pole (with age in Ma); there is, however, still significant uncertainty about the precise location of these poles (Smith 1999). Rotational movement of Gondwana is schematically shown by large curved arrow. *SB* = Sidney Basin.

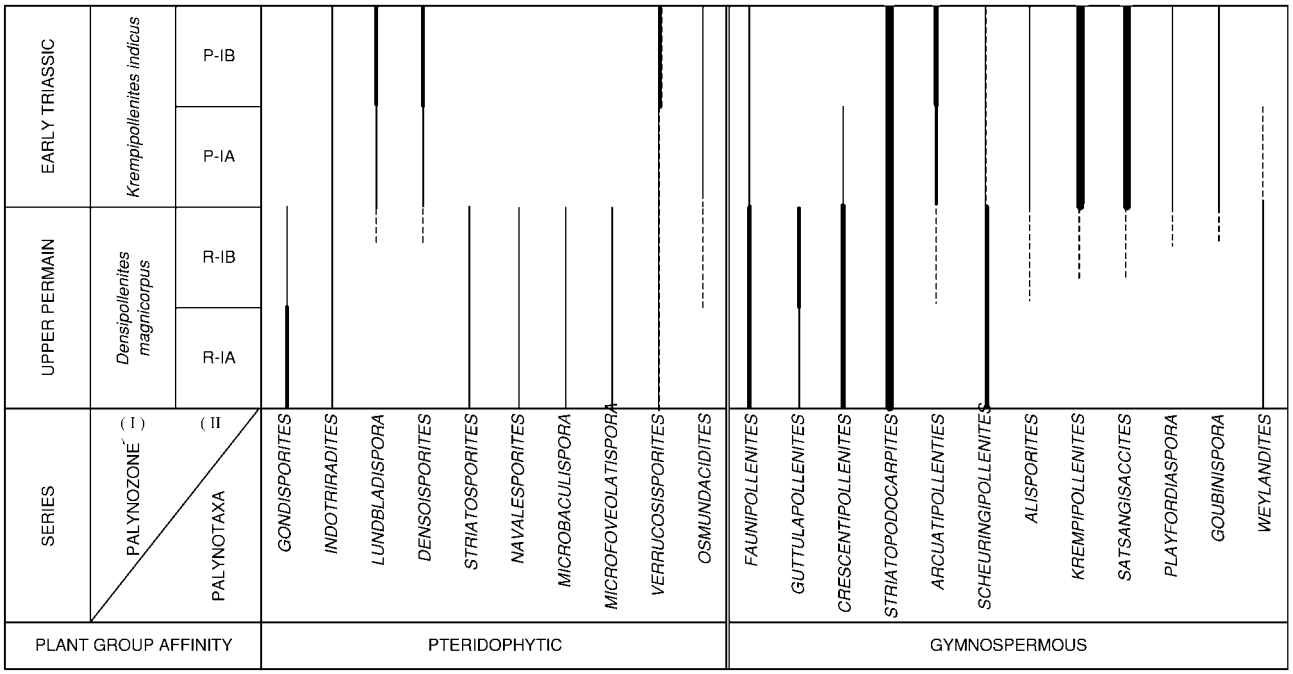

Figure 2. Generalized stratigraphic relative occurrences and first appearance of marker palyotaxa during the latest Permian and earliest Triassic in the Indian basins discussed in this article. Broken lines indicate the first intermittent occurrence. Thickness of solid line reflects relative quantitative continuous occurrence.

and it is not known if this light carbon originated in the oceans or in the atmosphere.

In a coupled atmosphere-ocean system, the carbon budget of the atmosphere is much smaller but more dynamic than that of the oceans, so that small oceanic perturbations are amplified significantly. The $\delta^{13}C$ stratigraphy of terrestrial sequences should, therefore, provide a more sensitive response and increased insights into the nature of these chemical excursions, despite the fact that terrestrial sequences are more likely to be discontinuous than marine sequences and, in general, have low biostratigraphic resolution. We have examined the carbon isotope signatures of organic remains of classic siliciclastic terrestrial Gondwana sequences from six basins of the former continental interior of Gondwana now preserved on three widely dispersed subcontinents to the south of its Tethyan margin (fig. 1)—South Africa, Madagascar, and India, all well known for rich preservation of fossil plants (Plumstead 1969; Wright and Askin 1987; Tiwari and Tripathi 1992; Tiwari 1996; Anderson et al. 1999). The details of the organic carbon isotope stratigraphy of these sequences, from Lower Carboniferous to Mid-Triassic, are reported elsewhere (Alexander 1999; Ghosh 1999; Rakotosolofo 1999; M. J. de Wit, J. Alexander, S. de Villiers, and S. Bowring, unpub. manuscript). Here we summarize $\delta^{13}C_{org}$ patterns across the paleontologically defined Permian-Triassic (P-T) boundaries of these sequences. The sequences in Madagascar were sampled along well-exposed river scarps; in South Africa, surface samples were analyzed and compared with previous studies of surface samples, fossils, and boreholes; in India, samples were obtained from 14 boreholes drilled in four different Gondwana basins. The palynological successions across the P-T boundary in India and in Madagascar are continuous and, particularly in India, well documented.

Palynofloral Changes across the Permian-Triassic Boundary

India. In our samples, the Late Permian palynoflora of India (fig. 2; table 1) is dominated by gymnospermous bisaccate pollen, namely, *Striatopodocarpites*, *Faunipollenites*, and *Crescentipollenites* with slight variation in the occurrence of other gymnospermous pollen *Guttulapollenites* and *Densi-*

Table 1. Summary of Organic Carbon Isotope Variations from Indian Gondwana Basins

Gondwana basin/ borehole	Stratigraphic interval	Isotopic characteristics
Damodar:		
RBM-1	13 samples from a 50-m-thick section across the P-T boundary	Three sharp negative excursions ($\delta^{13}C_{org} < -30$) interspaced by positive excursions ($\delta^{13}C_{org} > -25$) spanning ~20 m
RBM-3	15 samples from 640-m-thick section across the P-T boundary	A general decrease in the $\delta^{13}C_{org}$ value in the Upper Permian; at the P-T boundary is a sharp positive spike of ~3‰ followed by a negative spike of 7‰
R-14 and TDB-3	150 samples from an ~850-m-thick section from the top of glaciogenic Talcher Formation (Lower Gondwana) to the bottom of the Panchet Formation (Upper Gondwana)	At least two pronounced negative ($\delta^{13}C_{org}<-30$‰) spikes near the palynologically defined P-T boundary, one just below the boundary, the other ~50 m above it; in between these two negative spikes is a ~15-m-thick zone with highly positive $\delta^{13}C_{org}$ (~−16‰); total range of variation (from the most positive to the most negative value) across the P-T boundary is ~20‰); below the boundary are a number of cyclic repetitions of $\delta^{13}C_{org}$ values of ~3‰–4‰ superimposed on a background variation of ~1‰–2‰
RAD-5	11 samples across a 150-m section of the P-T boundary	Zone of pronounced negative $\delta^{13}C_{org}$ spikes (between −27 and −30) just above the palynologically defined P-T boundary; below and above this zone $\delta^{13}C_{org}$ value are ~24‰
RAD-6	10 samples across an ~25-m-thick section from across the P-T boundary	A large negative excursion ($\delta^{13}C_{org} < -30$‰) spanning ~5–10 m across the palynologically defined P-T boundary
RAD-8	10 samples across an ~16-m-thick section of the P-T boundary	$\delta^{13}C_{org}$ values of samples show three sharp negative spikes of ~4‰ interspaced by positive spikes; however, the total range is less in this section than in other sections
Mahanadi:		
TP-8	178 samples from a 1000-m section, from the top of the Talcher Formation (glaciogenic) in the lower part of the Gondwana sequence, to the middle part of the Kamthi Formation in the upper Gondwana sequence	These samples cover almost the entire Lower Gondwana sequence of peninsular India; most have $\delta^{13}C_{org}$ values between −26‰ and −23‰; three pronounced negative spikes ($\delta^{13}C_{org}$ value <−30‰) are within a span of ~60 m across the P-T boundary; the lowermost spike peaks just below the palynologically defined P-T boundary
TP-9	Nine samples from a 42-m section across the palynologically inferred P-T boundary	Two samples, one above the P-T boundary and the other below it, have $\delta^{13}C_{org}$ values <−28; other samples have $\delta^{13}C_{org}$ values between −20‰ and −26‰
TP-10	11 samples spanning an 82-m section across the palynologically inferred P-T boundary	A large negative incursion of ~5‰ is present ~10 m above the palynologically determined P-T boundary
Pranhita-Godavari:		
GAM-7	18 samples spanning a 224-m section across the palynologically inferred P-T boundary	A large (~8‰) negative spike is present ~10 m below the palynologically defined P-T boundary, followed by a strong positive $\delta^{13}C$ spike
GBR-7	14 samples spanning a 161-m section across the palynologically inferred P-T boundary	A 50-m-thick zone just above the P-T boundary has three negative spikes interspaced by positive spikes, but the large negative spikes normally associated with P-T boundaries could not be detected here
Warda coalfield:		
DGW-6	12 samples from 754 m across the palynologically defined P-T boundary	Very widely spaced samples make it difficult to detect any negative spike that might be present
Son Valley:		
UKD-8	11 samples from 160 m across the palynologically defined P-T boundary	There is no large negative spike associated with P-T boundary, only ~3‰ variation within this section

Note. See figure 1 for locations.

pollenites, and the lycopsid spore *Gondisporites*. The gymnospermous pollen continue to dominate the Lower Triassic palynoflora, too, but the assemblages are different from those of the Upper Permian. They are *Krempipollenites*, *Satsangisaccites*, *Arcuatipollenites*, *Lundbladispora*, *Playfordiaspora*, and *Striatopodocarpites* that are associated with the new group of lycopsid spores *Lundbladispora* and *Densoisporites*. The transition of palynoflora from Upper Permian to Lower Triassic shows a decline of species *Densipollenites indicus* and *Densipollenites invisus* and the disappearance of *Densipollenites magnicorpus*, *Gondisporites*, and the filicates *Navelesporites*, *Striatosporites*, *Microffaculispora*, and *Microfoveolatispora*. This transition is also associated with the appearance of *Arcuatipollenites pellucidus*, *Arcuatipollenites ovatus*, *Arcuatipollenites diffusus*, *Lundbladispora microconata*, *Lundbladispora brevicula*, *Densoisporites contactus*, *Playfordiaspora cancellosa*, *Satsangisaccites* spp., and *Krempipollenites indicus*. The change from the latest Permian to the earliest Triassic is distinct but gradual. The new components occur sporadically in the latest Permian palynoflora but firmly establish themselves during the lowermost Triassic and then flourish (fig. 2). More detailed palynofloral changes across the Indian P-T boundary and formal palynozones are described elsewhere (Singh and Tiwari 1982; Vijaya and Tiwari 1982, 1986; Tiwari and Singh 1983, 1986; Tiwari and Ram-Awatar 1987; Tiwari and Tripathi 1988, 1992; Srivastava and Jha 1990, 1995; Tiwari et al. 1992; Srivastava and Bhattacharyya 1996).

Madagascar. Our Upper Permian samples of the Madagascar sections contain a rich characteristic Lower Sakamena assemblage in which distinctive end-Permian pollen taxa *Weylandites striata* and *Guttulapollenites hannonicus* are abundant. Additional elements are *Leuckisporites virkkiae*, *Protohaploxypinus microcorpus*, *Weylandites lucifer*, *Dictyotriletes* sp., and *Apiculatisporis* spp. Younger samples contain an extremely poor but well-preserved Lower Triassic assemblage. It is marked with a sudden decline in the relative abundance of distinctive Upper Permian pollen taxa (*Weylandites, Lueckisporites,* and *Guttulapollenites*) and a concomitant increase of lycopsid spores, for example, *Densoisporites playfordii* and *Lundbladispora* sp. Further details of the palynofloral change across the P-T boundary are described by Goubin (1976) and Wright and Askin (1982).

South Africa. Pollen are poorly preserved in the southernmost part of the Karoo basin due to secondary alteration (see below). Here the P-T transition is based on vertebrates (Rubidge 1995; MacLeod et al. 2000).

Carbon Isotope Changes across the Permian-Triassic Boundary

Sampling and Analysis. In general, samples were collected at small (2–4 m or less) intervals. Samples with visible plant remains were preferentially separated for analysis. Where visible plant remains were not observed, dark gray or brown samples were preferred over pale-colored ones. About 0.5 mg of organic matter was used for the analyses. All samples were treated and analyzed using facilities at the University of Cape Town. Individual samples were cleaned with water to remove dirt that adhered to the samples. Small chips of each sample were visually inspected for carbonaceous remains. Where present, the carbonaceous matter in samples was collected with a surgical knife and kept in vials for further processing. Samples without visible carbonaceous matter were further ground to coarse grain sizes (~60 mesh) and inspected under a binocular microscope for visible finer-grained carbonaceous matter and collected for further processing. In samples where carbonaceous matters could not be separated in this way, a small (~1 g) portion of the sample was finely ground for further processing. Samples were immersed in dilute (1 : 6) HCl and kept in an oven at ~60°C for ~10 h to dissolve any carbonate that may have been present in the sample. Samples were finely ground to ensure that carbonates and bicarbonates were completely dissolved. After all the samples were treated with HCl, they were washed several times thoroughly with distilled water and then dried at ~60°C in an oven. Each dried sample was then inspected under a binocular microscope for final picking of the sample. For analyses in the automatic CN analyzer attached to a mass spectrometer, it is essential that the sample size remains within a narrow limit so that CO_2 obtained by oxidizing the sample is similar in quantity to the reference gas used for analyses. Larger- or smaller-sized samples do not yield precise analyses. Coal or carbonaceous shale samples weighing ~0.06 mg gave good results. For samples in which carbonaceous matter could be separated, physical description of each sample was noted. In samples where carbonaceous matter was not easily separated, enough bulk sample was prepared for analysis so that it contained ~0.06 mg of carbonaceous matter. Samples were packed within ~100 μL-sized tin microcapsules. All samples in this study were

analyzed with a Finnigan Mat 252 mass spectrometer fitted with an automatic CN analyzer with automatic sample loader. In this system, the sample is loaded in a tin vial that is burnt in the CN analyzer at ~1000°C. The resultant gas is passed through a dehydrant material and then through a gas chromatograph where CO_2 gas from the sample is separated from other gases. Separated CO_2 gas is then passed to the mass spectrometer for isotopic analyses. An internal standard was first calibrated using NBS-21 standard, and one internal standard was analyzed alternately with almost every five samples. Sample preparation of carbonate nodules (which ranged from 5 to 10 cm across) began with a cleaning of the samples to remove the modern carbonaceous material adhering to the surface. Each nodule was cut and the outer surface was removed to avoid contamination from possible penetrating modern roots and/or algae. Samples of ~2 g from the inner part were cleaned with distilled water. The fine carbonaceous material within the nodules was crushed and finely ground for further processing. The powdered bulk samples were immersed in dilute HCl (1 : 6) and stirred occasionally to ensure complete dissolution of inorganic carbon. Both cold and warm HCl were used to remove both calcium carbonates and dolomite. When effervescence resulting from acid digestion of calcium carbonates stopped, the samples were put in a fresh acid bath for 12 h to allow complete digestion of dolomite and the remaining calcium carbonates. After acid treatment, each sample was washed with distilled water to remove excess HCl and calcium salts; acid digestion and washing were repeated several times until no reaction occurred when fresh acid was added. When the carbonate dissolutions were completed, the damp samples were dried at 80°C until excess water evaporated. The oven-dried samples were weighed and sealed into 5 × 3.5-mm tin capsules. A sample in the amount of 20 mg was packed into the tin capsule for analyses. Analysis was carried out as described above.

Organic Carbon Isotope Patterns. In peninsular India, 470 samples were analyzed from 14 different boreholes across four coal-bearing subbasins. The results are summarized in figure 3 and table 1. Out of six boreholes in the Damodar Valley coal basin, five boreholes (RAD-5, RAD-6, R-14, RBM-1, and RBM-3) intersected the palynologically inferred P-T boundary (fig. 6). Permian values oscillate between −26‰ and −22‰, averaging −24‰. Such oscillations, which we record throughout the terrestrial Gondwana basins, are probably due to local climate fluctuations, eustatic factors, and weathering, as well as differential isotopic fractionation within biomes and between different parts of individual plants (Smith et al. 1976; De Niro and Hastof 1984; Tieszen 1991; van der Merwe and Medina 1991; Schlesser 1992; White et al. 1994; Cerling et al. 1997; Gröcke et al. 1999). Close to the P-T boundary, sharp negative $\delta^{13}C_{org}$ spikes with values more negative than –28‰ and –34‰ were detected in four of these boreholes (RAD-5, RAD-6, RBM-1, and R-14). Zones of negative spikes, separated by sharp reversals, span thicknesses between ~20 m (RBM-1) and ~40 m (RAD-5). A negative excursion of ~12‰ occurs directly below the P-T boundary in borehole R-14. This negative spike is rapidly followed by a distinct positive excursion of ~21‰ to −16‰. All three boreholes from the Mahanadi Valley coal basin (TP-8, TP-9, and TP–10, Talcher coalfield; fig. 3) intersected the palynologically defined P-T boundary. Both TP-8 and TP-10 show large and well-defined negative $\delta^{13}C$ excursions around this boundary, following a regular pattern of oscillations of ~2‰–3‰ around −25‰ throughout the Permian. In TP-9, the palynological P-T boundary is not well defined. Triassic palynoflora exist at least up to 280.5-m borehole depth (fig. 6). One sample at 317 m depth yielded a $\delta^{13}C_{org}$ value of −30‰. This may be related to the P-T spikes, but this is not certain. In TP-10 the sharp negative excursion is present within ~10 m above the palynologically inferred P-T boundary. In the TP-8 borehole, three sharp negative excursions associated with the P-T boundary span a borehole depth of ~60 m. The first negative excursion (>6‰) occurs below the P-T boundary, while two subsequent negative excursions (~8‰ and 11‰) occur well above the P-T boundary. Out of the three boreholes from the Pranhita-Godavari coal basin (GAM-7, GBR-7, and DGW-6, Wardha and Godavari coalfields; fig. 3) and one from the Son Valley coal basin (UKD-8, Korar coalfield; fig. 2), only GAM-7 shows a sharp large negative spike of ~9‰, followed by a sharp reversal of ~14‰. In the samples from the other boreholes, no regular patterns of variation across the P-T boundary were detected beyond those of general background oscillations (fig. 3; table 1). In several sections, the $\delta^{13}C$ values recover in the Triassic to near Upper Permian values, but the oscillations around the mean Triassic values are clearly greater and less regular (fig. 3).

In southern Madagascar, 150 samples were collected for analysis in the Morondava basin; here the Gondwana sequence unconformably overlies Precambrian basement (Rakotosolofo 1999). Carbon isotope stratigraphy between different sections compare well, and large, positive $\delta^{13}C_{org}$ spikes in the Carboniferous–Lower Permian glacial sequences

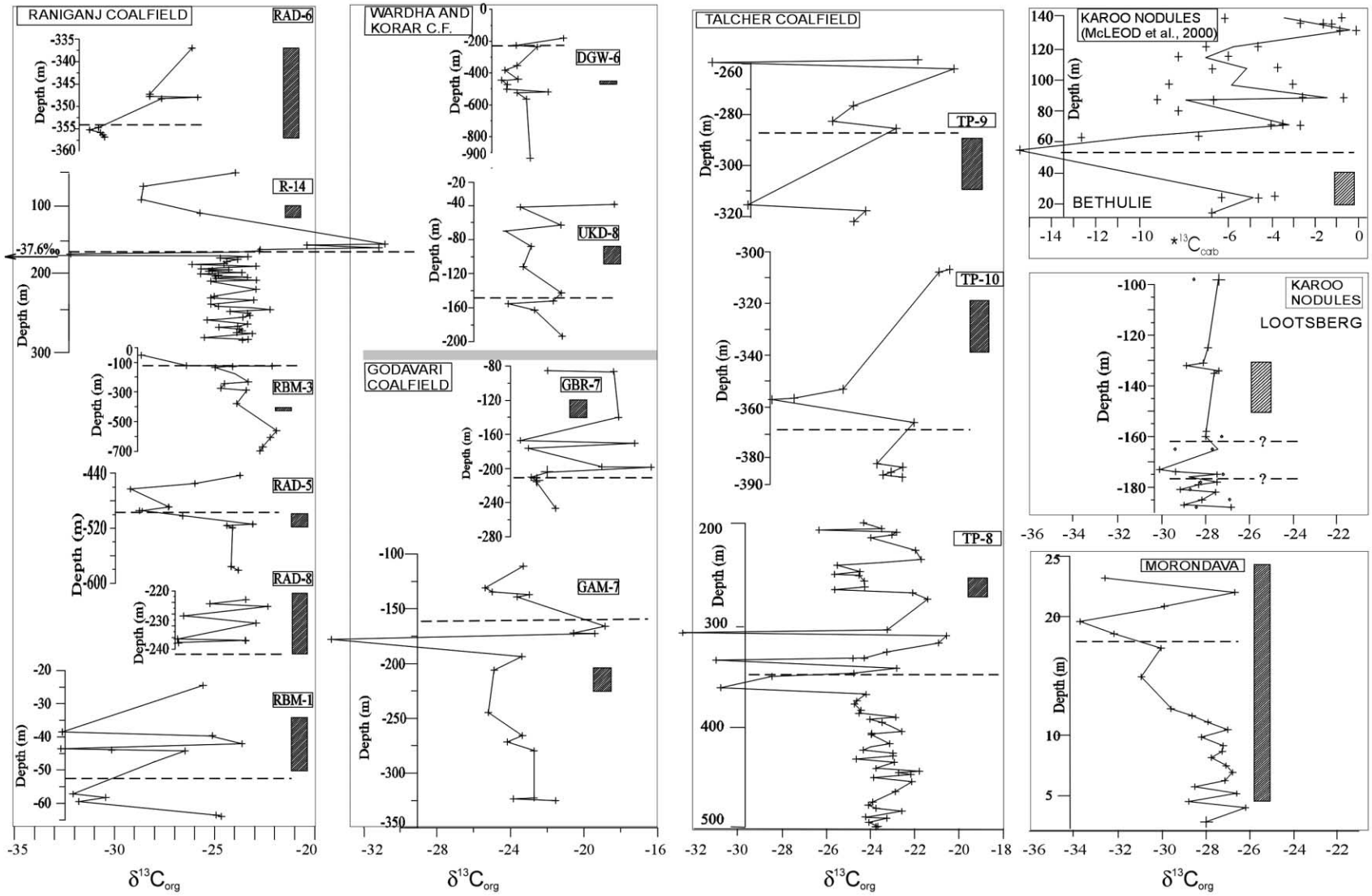
RANIGANJ COALFIELD
RAD-6
R-14
-37.6‰
RBM-3
RAD-5
RAD-8
RBM-1
WARDHA AND KORAR C.F.
DGW-6
UKD-8
GODAVARI COALFIELD
GBR-7
GAM-7
TALCHER COALFIELD
TP-9
TP-10
TP-8
KAROO NODULES (McLEOD et al., 2000)
BETHULIE
KAROO NODULES
LOOTSBERG
MORONDAVA
Depth (m)
δ13Corg
δ13Ccarb

can be correlated with confidence (Rakotosolofo 1999; N. Rakotosolofo, M. J. de Wit, and L. D. Ashwal, unpub. data). A steady decrease of 4‰ in the average $\delta^{13}C$ of ~26% (against frequent background $\delta^{13}C$ fluctuations of ~2‰) is clearly evident throughout the Upper Permian (fig. 3). Closely spaced samples across the Permo-Triassic boundary delineate a large sharp negative $\delta^{13}C$ spike (~6‰). The onset of this negative excursion starts in the uppermost Permian but does not reach its peak at −34‰ until the lowermost Triassic. A second negative peak (~6‰) in the Lower Triassic follows a sharp positive reversal of ~8‰ (fig. 3).

In South Africa, attempts to record the $\delta^{13}C_{org}$ across the P-T boundary of the Gondwana sequence (the Karoo Supergroup) have yielded contrasting results. A gradual negative trend leading up to the P-T boundary was recorded from different parts of this extensive basin using apatite from tusks of the mammal-like reptile *Dicynodon* (as a proxy for the contemporaneous vegetation of these herbivores) and organic carbon from boreholes through coal-bearing sequences, respectively (fig. 1; Thackeray et al. 1990; Faure et al. 1995). Both these studies conclude that the start of a gradual decline in $\delta^{13}C$ of ~10‰ was well on the way before the P-T boundary, but a lack of appropriate fossil material and absence of coal prevented further analysis across the P-T boundary. A subsequent third study of carbonates from diagenetic nodules and vertebrate tusks (MacLeod et al. 2000) conducted at three further sites in the southern and central part of the Karoo basin (Doornplaats, Lootsberg, and Bethulie, respectively; fig. 1) gave conflicting results. At Doornplaats and Lootsberg, for example, no discernible spike was detected and no change was recorded in the $\delta^{13}C_{carb}$ leading up to the P-T boundary. This was attributed to possible diagenetic alteration (MacLeod et al. 2000) but is more likely related to synorogenic basinal fluid activity between ~278 and 247 Ma (see below). At Bethulie, however, a marked shift of ~10‰ in $\delta^{13}C_{carb}$ of carbonate nodules is recorded close to the P-T boundary (fig. 3). The onset and decline of the negative $\delta^{13}C$ peak spans more than 15 m within which both Permian (*Dicynodon*) and Triassic (*Lystrosaurus*) vertebrates co-occur. Depending on the sedimentation rates applied to this rapidly changing environment from meandering to braided rivers (Ward et al. 2000), the minimum duration of the $\delta^{13}C$ spike is greater than 1 million years. Thus, the $\delta^{13}C$ event at Bethulie was neither geologically nor biologically instantaneous (MacLeod et al. 2000).

Interpretations of the $\delta^{13}C$ from samples closer to the southern margin of the Karoo basin are less reliable because of the proximity to the Cape Fold Belt and the southern active convergent margin of Gondwana (fig. 1). The Cape Fold Belt formed between ~278 and 247 Ma (Hälbich et al. 1983) as part of an extensive orogenic belt along the southern periphery of Gondwana (Trouw and de Wit 1999; Turner 1999). Basinal fluids rich in CH_4-CO_2 were tectonically driven away from the emerging Cape Fold Belt through the Karoo basin, up to at least 50 km ahead of the present-day exposures of the Cape Fold Belt thrust front (Egle 1996; Egle et al. 1998). In this region, fluid inclusion studies on vein material from the Karoo Supergroup, up to and including the uppermost Beaufort Group, display general homogenization temperatures around 150°–170°C, and locally as high as 270°C. Hydrogen and oxygen isotope analysis on fluid inclusions of vein-quartz implicate a mixture of meteoric water with fluids generated by dehydration reactions and devolatilization during low-grade metamorphism (Egle 1996; Egle et al. 1998). Carbon isotope analysis on calcite from veins and adjacent host rock shows, however, that the fluid system in the Karoo basin was rock buffered on the scale of individual lithostratigraphic units. There is a large scatter in $\delta^{13}C_{carb}$ of vein calcite (−18.7‰ to +8.5‰ PDB) and host rocks carbonate (−8.4 to +6.1‰ PDB). Carbon isotope measurements nevertheless record local equilibrium conditions between vein calcite and

Figure 3. Variations in organic carbon isotope ratios across the palynologically defined Permian-Triassic boundary (*broken lines*). Note the large negative multiple excursions before and after the boundary, separated in places by significant positive excursions. All basins display relative "steady-state" Carboniferous and Permian signatures around −25‰ (Ghosh 1999; Rakotosolofo 1999; M. J. de Wit, J. Alexander, S. de Villiers, and S. Bowring, unpub. manuscript). The large-amplitude perturbations near the P-T boundary disappear only gradually in the Middle Triassic. In the Indian basins, the palynological P-T transition is sharp in boreholes TP-8, RAD-5, UKD8, and DGW-6. Palynological changes in other Indian boreholes are abrupt and indicate a break (fig. 6). A sharp palynological transition is also observed in the Morondava Basin of Madagascar. In the Karoo Basin, South Africa, palynology is hampered by secondary alteration; instead the P-T transition is based on vertebrate paleontology, with a poor resolution across a broad zone (≥1 m.yr.; MacLeod et al. 2000). For comparison, $\delta^{13}C_{carb}$ variations are also shown (*upper right*; modified from MacLeod et al. 2000). Scale bars (*diagonal hatch*) = 20 m.

host rock carbonate, and two samples of vein calcite in the Beaufort Group closest to the P-T boundary yield $\delta^{13}C_{carb}$ PDB of −16 and −10 ‰, similar to that of diagenetic calcite across the P-T boundary (−18 to −12‰) at Doornplaats, a locality within the range of paleofluid migration associated with the Cape Fold Belt orogeny (fig. 1). These values also overlap with those of calcite from diagenetic nodules that range from −4‰ to −11‰ (MacLeod et al. 2000). A similar range of $\delta^{13}C$ values of carbonate and sparry calcite (−2‰ to −18‰) is recorded across the P-T boundary nearby, at Lootsberg (MacLeod et al. 2000; K. MacLeod, unpub. data). Thus, secondary alteration has significantly influenced the $\delta^{13}C$ of calcite across the P-T boundary of the southern sections of the Karoo basin of South Africa. Farther north (Bethulie) and in the coalfields along the northern margin of the Karoo basin, these alterations are less significant (Faure et al. 1995; MacLeod et al. 2000), corroborating the influence of the CH_4-CO_2 rich basinal fluid flow in the coarse clastic sediments of the Upper Permian and Lower Triassic close to the orogenic front of the Cape Fold Belt. This is also borne out by widespread remagnetization and generally poor preservation of primary paleomagnetic signatures of the lower Beaufort Group (Upper Permian to Lower Triassic) of the Karoo of this region, while those closer to the tectonic front in the upper Beaufort (Middle Triassic—i.e., postdating fluid migration) are extremely stable (Ballard et al. 1986; Opdyke et al. 2001).

The secondary alterations recorded in $\delta^{13}C$ of carbonates of coarse-grained clastics have had less effect on $\delta^{13}C$ of organic materials of fine-grained rocks, even those close to the orogenic front of the Cape Fold Belt, where alteration temperatures reached 150°C. Here, significant well-preserved $\delta^{13}C_{org}$ excursions (>10‰) can be correlated between lithostratigraphic sections separated along strike by more than 500 m (Ghosh 1999; Faure and Cole 1999). Therefore, we separated organic matter preserved in 30 soil carbonate nodules collected at Lootsberg across the P-T boundary. The $\delta^{13}C_{org}$ shows significant fluctuations in the Upper Permian between −27‰ and −29‰, and a small negative spike (−30‰) is discernible (fig. 3) around the P-T boundary. Lack of nodules throughout the section prevents us from possibly identifying more pronounced spikes. However, there is a significant negative trend in the δC_{org} from a mean around −23‰ between ~260 and 270 Ma (M. J. de Wit, J. Alexander, S. de Villiers, and S. Bowring, unpub. manuscript) to a mean around −28‰ closer to the P-T boundary (fig. 3). This complements similar findings of earlier research (Thackeray et al. 1990; Faure et al. 1995).

An Interactive Systems Model for Changes across the Permian-Triassic Boundary. The Permo-Triassic carbon isotope stratigraphy from the terrestrial basins of Gondwana clearly complements that of the marine sections from the peripheral margins of Gondwana and farther afield in Laurentia (Looy 2000; Twitchet et al. 2001). This implicates a coupled atmosphere-ocean system. To test some likely scenarios that have been proposed to account for the observed changes across the P-T boundary, we use a global carbon-flux model in which the ocean is coupled to changes in the atmosphere via the silicate continental weathering flux, and the atmosphere to changes in the ocean via the residual of the ocean-atmosphere CO_2 flux (fig. 4). Changes in the magnitude of fluxes are prescribed to allow a first-order evaluation of the magnitude of the ocean-atmosphere response to particular perturbations compared to observations and the feedback processes required to counterbalance these perturbations.

The transient model of the carbon cycle of the atmosphere (C_{atm}, $^{12}C_{atm}$, or $^{13}C_{atm}$) and ocean (C_{ocean}, $^{12}C_{ocean}$, or $^{13}C_{ocean}$) can be summarized by two simple equations:

$$\frac{dC_{atm}}{dt} = F_{ocean} + F_{oxidCorg} + F_{CH4} + F_{volc} - F_{C3} - F_{C4} - F_{weath}, \quad (1)$$

$$\frac{dC_{ocean}}{dt} = F_{riv} + F_{mantle} + F_{CH4} - F_{CaCO3} - F_{orgC} - F_{basalt}. \quad (2)$$

The subscripts refer to the fluxes summarized in figure 4. The ocean-atmosphere exchange flux is modeled as a residual flux F_{ocean}, and equilibrium exchange is not assumed. The isotope fractionation factors between reservoirs are assumed to be constant and incorporated as proportionality constants in the fluxes above to calculate $d^{12}C/dt$ and $d^{13}C/dt$ and from that $d\delta^{13}C/dt$. All fluxes are held constant except where specified, in which case the transient response $\delta C_{atm}/dt$ and $\delta C_{ocean}/dt$ following prescribed stepwise changes in flux magnitudes are calculated. Neither C_{atm} or C_{ocean} is held constant. The time step is 100 yr, smaller than the residence time of atmospheric CO_2 with respect to the residual of the ocean-atmosphere exchange flux, to ensure stability. Changes in C_{atm} are coupled to dC_{ocean}/dt via the F_{ocean} term in equation (1), and

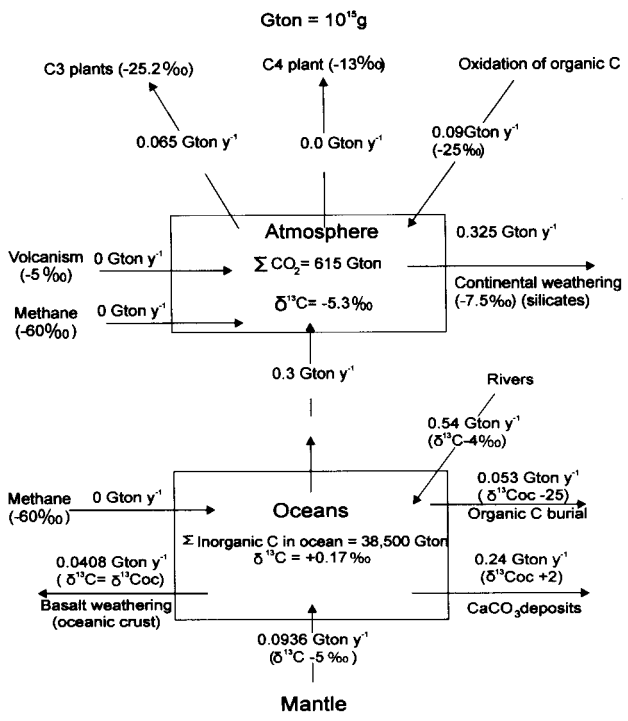

Figure 4. Coupled atmospheric and oceanic carbon budget (based on present-day reservoirs and assuming mass balance, e.g., "exchangeable reservoirs," but excluding fossil fuel CO_2 addition). Carbon flux magnitudes, the $\delta^{13}C$ composition of reservoirs, and isotope fractionation factors between reservoirs ($\Delta\delta^{13}C$) are from Arthur (2000) and represent the present steady-state ocean-atmosphere environment. Fractionation factors between reservoirs are held constant. Magnitude of fluxes changes only when prescribed, e.g., CH_4 pulse in figure 5*A*; C3 biomass to C4 biomass in figure 5*B*; and mantle and C3 biomass fluxes in figure 5*C*. In figure 5*A*, atmospheric CO_2 is allowed to increase in response to the CH_4 flux, and feedbacks, such as possible increased biomass production or continental weathering, are not prescribed. y = year.

dC_{ocean}/dt is coupled to dC_{atm}/dt via the silicate fraction of the F_{riv} term in equation (2). (The implicit assumption is that the carbonate weathering component is constant.) In this simple model, fluxes such as F_{weath} are held constant unless otherwise stated, and no functional dependence on C_{atm} is assumed. Such functionalities probably exist but are excluded in this model to allow for a first-order evaluation of the system response to specific perturbations in the absence of complicating feedback processes.

Modeling scenarios of Upper Permian to Lower Triassic events, in concert with the carbon isotope stratigraphy, must take into account:

1. The changing paleogeography of the supercontinent Pangea and, in particular, the rotation of Pangea, following the earlier drift of the Gondwana sector away from polar latitudes (fig. 1). The marine platforms flanking the northern margin of Gondwana from which many of the marine carbon isotope sections have been recorded (Baud et al. 1989) changed their positions from temperate to tropical positions. In contrast, the terrestrial basins investigated in this study (and others such as the Sydney basin [Retallack 1999; fig. 1]) remained at relatively high latitudes during the P-T transition (50°–75°S). In addition, repositioning of the continents was accompanied by general global warming (although earth may not have been entirely free of northern polar ice; Beauchamp 1994) and changes in ocean dynamics (Veevers et al. 1994; Knoll et al. 1996; Isozaki 1997; Retallack 1999; Scotese et al. 1999; Scotese 2000; Zhang et al. 2001).

2. The northern continental marine platform of Gondwana became unstable in Middle Permian times (~260–270 Ma) and disintegrated into a number of smaller fragments that then dispersed to collide along the southern Laurasian margin (fig. 1; Smith 1999; Scotese 2000). An episode of increased length of seafloor spreading-ridge must have accompanied the formation and translation of these microcontinents.

3. A significant but gradual eustatic drop in sea level throughout the Permian followed by a sharp minimum near the P-T boundary (Hallam 1992, 1998; Erwin 1993). There is considerable debate about the precise timing of the P-T sea level lowstand, in part because it is not clear to what extent the change in sea level is truly eustatic or related to local tectonics (Dickens 1992; Hallam and Wignall 1997). For example, it is counterintuitive to relate a drop in sea level during the end Permian to eustatic changes, given extensive global deglaciation in the Permian (Scotese 2000). It is probable, therefore, that the relative drop in sea level is related to increased global tectonism (Dickens 1992; Faure et al. 1995; Hallam and Wignall 1997; Scotese 2000) and specifically thermal uplift and rifting of the continental margin of NE Gondwana before its breakup and the start of seafloor spreading during the opening of Tethys. The former would rapidly have been succeeded by relative rise of local sea level across the rifted fragments; the latter would have enhanced eustatic sea level rise.

4. A drop in the ratio of $^{87}Sr/^{86}Sr$ of seawater in Middle-Upper Permian times (~275–250 Ma) followed by a sharp rise of this ratio in the Lower-Middle Triassic (250–225 Ma; Veizer et al. 1999). This signals a relative increase/decrease in ratio of

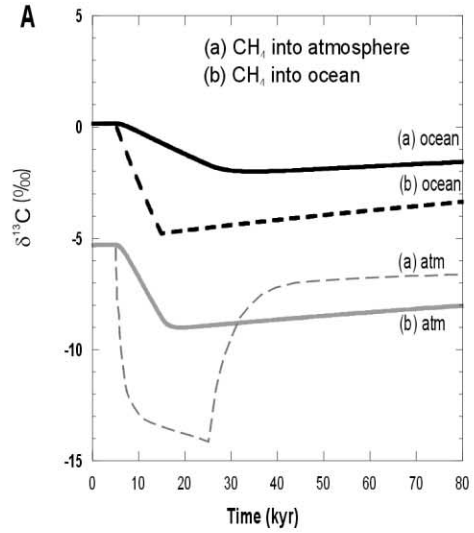
A
(a) CH_4 into atmosphere
(b) CH_4 into ocean
(a) ocean
(b) ocean
(a) atm
(b) atm
$\delta^{13}C$ (‰)
Time (kyr)

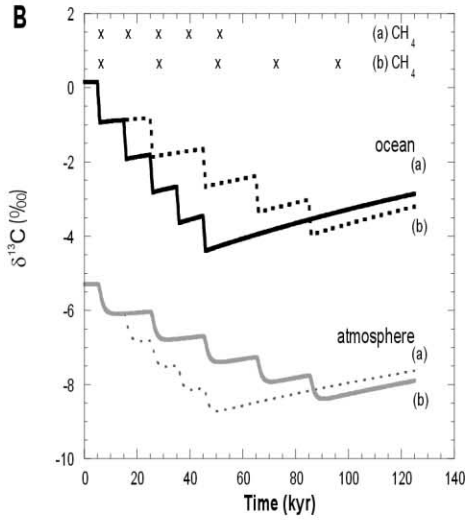
B
(a) CH_4
(b) CH_4
ocean
(a)
(b)
atmosphere
(a)
(b)
$\delta^{13}C$ (‰)
Time (kyr)

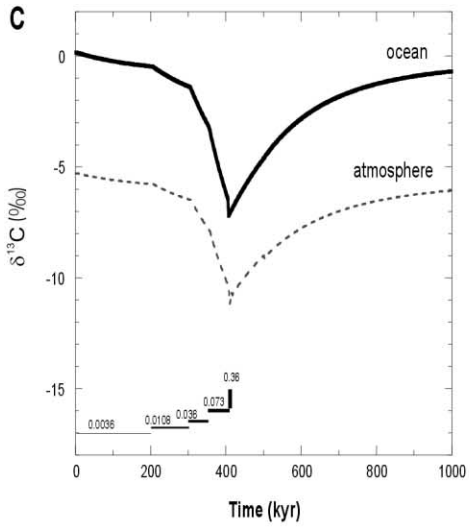
C
ocean
atmosphere
0.0036
0.0108
0.036
0.073
0.36
$\delta^{13}C$ (‰)
Time (kyr)

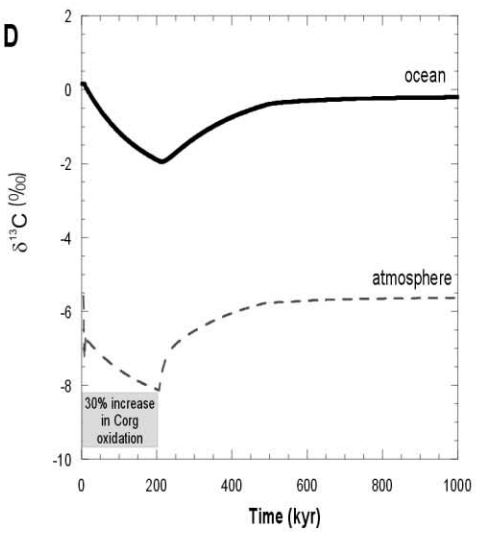
D
ocean
atmosphere
30% increase in Corg oxidation
$\delta^{13}C$ (‰)
Time (kyr)

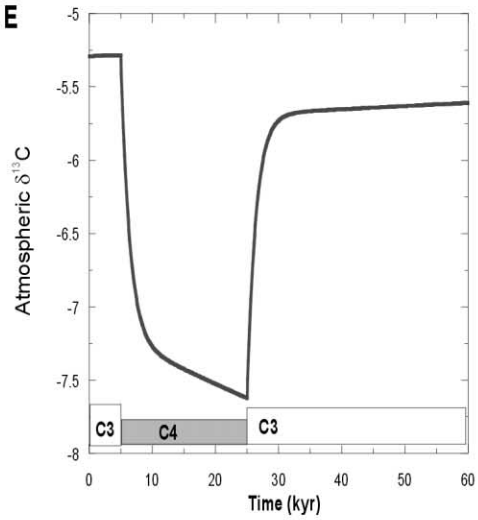
E
C3
C4
C3
Atmospheric $\delta^{13}C$
Time (kyr)

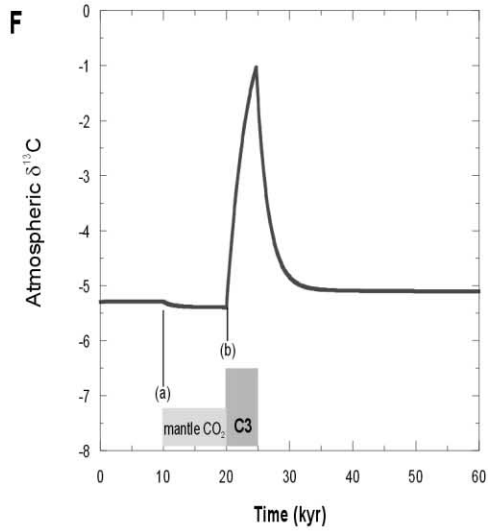
F
(a)
(b)
mantle CO_2
C3
Atmospheric $\delta^{13}C$
Time (kyr)

ocean floor weathering to continental weathering and runoff, respectively (Edmond 1992).

5. Outpourings of one of Earth's largest flood basalts (Siberian volcanic province) starting at ~251 Ma (Renne et al. 1995; Kamo et al. 1996; Bowring et al. 1998). The Siberian Flood Basalts have been dated with high precision using Ar/Ar and U/Pb isotopes. While the results are not all directly com-

Figure 5. *A*, Response of $\delta^{13}C_{atm}$ and $\delta^{13}C_{ocean}$ to CH_4 pulses introduced into the ocean-atmosphere system. *a*, Curves illustrate a CH_4 pulse injected directly into the atmosphere. The model time step is 100 yr, equivalent to the residence time of atmospheric CO_2 with respect to the ocean-atmosphere exchange flux. A longer time step (1000 yr) "saturates" the atmosphere and results in rapid excursions immediately following perturbations, followed by the trends observed using the smaller time step. The $\delta^{13}C_{atm}$ and $\delta^{13}C_{ocean}$ curves in *b* illustrate the effect of a rapid CH_4-hydrate pulse directly into the ocean (rate of 0.36 Gton C/yr over 10,000 yr, representing an integrated CH_4 flux equivalent to 24%–48% of the present global clathrate reservoir). The result is a −5‰ shift in $\delta^{13}C_{ocean}$ and a ~−4‰ shift in $\delta^{13}C_{atm}$ (the latter is associated with the more negative $\delta^{13}C$ of the ocean-to-atmospheric flux itself, with the flux magnitude maintained constant). This model result implies that about one-third of the negative $\delta^{13}C_{atm}$ excursion across the P-T boundary can be attributed to the change in the $\delta^{13}C$ of the ocean-to-atmosphere flux itself, without any change in flux magnitudes. If all of a −12‰ excursion in $\delta^{13}C_{atm}$ is attributed to CH_4 released into the ocean, this will require that ~5% of the CH_4 released into the ocean (calculated above) escapes to the atmosphere; this will increase the atmospheric CO_2 concentration by 28%, to about 370 ppm. *B*, Response of the ocean and coupled atmosphere to five CH_4 pulses of 0.72 Gton C/yr (for 1000 yr at a time) spaced out at (*a*) 10,000-yr and (*b*) 20,000-yr intervals. Longer intervals between pulses allow the system more time to return toward "steady-state" values; the negative shift in $\delta^{13}C_{ocean}$ and $\delta^{13}C_{atm}$ is more gradual and slightly smaller. *C*, Response of the ocean and coupled atmosphere to the gradual release of CH_4 (directly into the ocean) building up to a large rapid pulse over 400,000 yr: 0.0036 Gton C/yr over the first 200,000 yr, followed by increases to 0.0108 Gton/yr sustained for 100,000 yr, 0.036 Gton/yr and then 0.073 Gton/yr for 50,000 yr each, and eventually a rapid 0.36 Gton/yr flux for 2000 yr. The total CH_4 released over 400,000 yr is equivalent to 50%–100% of the present clathrate reservoir size. Only a small (<5%) fraction of the CH_4 released into the ocean has to escape to the atmosphere, in addition to the already established ocean-to-atmosphere CO_2 flux, to provide the larger $\delta^{13}C_{atm}$ than $\delta^{13}C_{ocean}$ excursions seen in preserved organic and carbonate carbon. *D*, Atmosphere response to increased flux of terrestrial organic carbon oxidation. The rate of organic carbon oxidation is increased by 30% relative to the 0.09 Gton/yr in the present budget (fig. 3) and sustained for 200,000 yr to simulate the response of $\delta^{13}C_{atm}$ to increased oxidation of, for example, the Permian coal (Faure et al. 1995). The $\delta^{13}C_{atm}$ declines to ~2.5‰ lower than the present and then increases again as the output functions forces it to the steady-state scenario. This increased organic carbon oxidation will result in very high atmospheric CO_2 levels that will have to be removed into a reservoir with a $\delta^{13}C$ value close to that of the atmosphere for it not to result in additional $\delta^{13}C$ excursion trends (e.g., continental weathering as opposed to increased C3 production). This mechanism on its own cannot produce the sharp negative $\delta^{13}C_{org}$ spikes found at the P-T boundary; however, the rapid overlapping rise of $^{87}Sr/^{86}Sr$ in the early Triassic is compatible with sharp increase in continental weathering and the input of orogenic uplift. *E*, Response of the system to switches between C3 and C4 terrestrial plants. A sudden switch from C3 to C4 terrestrial biomass production and therefore burial (at $t = 5000$ yr; all flux magnitudes constant, including total C going into C3-C4 reservoir) results in a rapid negative shift in atmospheric $\delta^{13}C$ of ~2‰. If C4 production is maintained (from 5000 to 25,000 yr), it trends toward a new $\delta^{13}C_{atm}$ "steady-state" scenario with more negative $\delta^{13}C_{atm}$ (all flux magnitudes and isotope fractionation factors assumed constant; the only variable is the changing isotope composition of fluxes from the atmosphere in response to $\delta^{13}C_{atm}[t]$). A sudden switch back to C3 terrestrial biomass (again all flux magnitudes and fractionation factors constant), produces a fast positive atmospheric $\delta^{13}C$ excursion of ~2‰, with the eventual "steady-state" $\delta^{13}C_{atm}$ value more positive than during C4 plant production. This is compatible with the $\delta^{13}C_{org}$ patterns observed in several of the Indian basins (R-14, GAM-7, and TP-8 and -9); however, C3 to C4 switches are probably associated with variations in atmospheric CO_2 levels (at threshold values of about 500 ppm; Cowling 1999) brought about by processes that may offset or cancel the trends discussed above (see *C*). *F*, The response of the system to increased mantle CO_2 and coupled C3 biomass production. The sharp positive spikes in $\delta^{13}C_{atm}$ following the negative excursions may be the result of increased terrestrial biomass production and burial (C3 in this example) triggered by elevated atmospheric CO_2 levels associated with, for example, volcanism from the outpouring of Siberian platform basalt (and/or CH_4 release). Illustrated is the response of $\delta^{13}C_{atm}$ to (*a*) an increased flux of mantle CO_2 to the atmosphere ($\delta^{13}C$ of −6‰, sustained for 10,000 yr at a rate of 0.065 Gton C/yr, equivalent to present biomass production rate). This scenario produces a negligible excursion in $\delta^{13}C_{atm}$ but an almost doubling of atmospheric CO_2 levels to 570 ppm in 10,000 yr, at which point (*b*) terrestrial C3-biomass production rates are increased by a factor of 2.5, which results in a rapid, large, positive excursion in $\delta^{13}C_{atm}$. This increased biomass production is sustained until atmospheric CO_2 levels fall below 400 ppm (i.e., for 5000 yr). The change in $\delta^{13}C_{ocean}$ associated with this rapid positive excursion in $\delta^{13}C_{atm}$ is <0.5‰.

Series	Palynozone I	Palynozone II	Borehole	TP-8 (1)	TP-9 (2)	TP-10 (3)	RAD-2 (4)	RAD-5 (5)	RAD-6 (6)	RAD-8 (7)	UKD-8 (8)	DGW-6 (9)	GAM-7 (10)	GBR-7 (11)
Lower Triassic	*Playfordiaspora cancellosa*		P-IV B	307.30 - 334.00										
			P-IV A											166.00
			P-III B		259.00 - 280.50	338.00 - 352-80	460.00							
			P-III A						355.20				214.00	
			P-II B											
			P-II A											
	Krempipollenites indicus		P-I B							210.50				
Upper Permian			P-I A	367.50				510.00			41.50 - 69.70	182.50		
	Densipollenites magnicorpus		R-I B	374.00 - 404.00	318.09 - 649.63	385.00	450.00	512.00	396.10	370.50	152.30	226.15	217.75	178.45
			R-I A											

Figure 6. Composite table showing the palynological assemblages identified at various depths (m) in some of the Indian borecores used in this study. Stippled area indicates discontinuity in the palynoflora. (*I*) Tiwari and Tripathi 1992; (*II*) Tiwari and Singh 1986; (*1*) A. Tripathi, unpub. data ; (*2, 3*) A. Tripathi, personal observation; (*4*) Singh and Tiwari 1982; (*5*) Tiwari and Singh 1983; (*6, 7*) Tiwari et al. 1992; (*8*) Tiwari and Ram-Awatar 1987; (*9*) Srivastava and Bhattacharya 1996; (*10*) Srivastava and Jha 1990; (*11*) Srivastava and Jha 1995.

parable, the onset of the volcanism is older than 251.2 ± 0.3 Ma (Kamo et al. 1996), a date indistinguishable from the date of the negative $\delta^{13}C$ peak in China (251.4 ± 0.3 Ma) and, thus, within error of the P-T boundary of the marine sequences (Bowring et al. 1998). However, it is not known how long the volcanism may have lasted; a time span of 1–3 million years (~251–248 Ma) is a reasonable estimate given the stratigraphic and geochronologic uncertainties (Renne et al. 1995). The absolute relationship between the volcanic emissions and the major extinctions still requires accurate dating across the entire 3.5-km-thick basalt sequence.

6. Relatively high P_{CO_2}/low P_{O_2} of the atmosphere during the Permo-Triassic Transition (Berner 1994; Graham et al. 1995; Ekart et al. 1999; Berner et al. 2000; D. H. Rothman, unpub. manuscript), and relative anoxic conditions in the deep oceans (Kajiwara et al. 1994; Knoll et al. 1996; Hallam and Wignall 1997; Isozaki 1997; Hottinski et al. 2001; Zhang et al. 2001).

Our observations are consistent with recent models that link other large negative $\delta^{13}C$ excursions in the Phanerozoic rock record to a massive release of methane stored as solid CH_4-hydrates (clathrates) on the continental margins (Dickens et al. 1995; Hesselbo et al. 2000; Kennett et al. 2000; Krull and Retallack 2000; Krull et al. 2000; Padden et al. 2001). These gas hydrates are metastable, and both increased temperature and decreased pressure destabilizes the CH_4-ice, leading to liberation of stored gas (Kvenolden 1998; Max 2000). The very negative $\delta^{13}C$ value of this methane (average ~−60‰, with values as low as −120‰; Kvenolden 1988, 1993) provides an obvious source with which to produce negative $\delta^{13}C$ excursions in both the oceans and the atmosphere (fig. 5*A*), as first suggested by Erwin (1993). The model response indicates that a flux of 0.065 Gton C/yr (equivalent to the CO_2 buried as terrestrial biomass at present) is introduced and then maintained for 20,000 yr (equal to 1300 Gton C, or 9%–18% of the present

CH_4 hydrate reservoir), and it produces a rapid −8‰ shift in $\delta^{13}C_{atm}$. Atmospheric CO_2 increases in response to this prolonged CH_4 pulse are as follows: levels double after 10,000 yr, and when the CH_4 flux is terminated after another 10,000 yr, atmospheric CO_2 is about 900 ppm, about three times the original value (290 ppm), if all other flux magnitudes remain constant. After the initial rapid negative change in $\delta^{13}C_{atm}$, continued introduction of CH_4 results in a new "isotopic steady-state" (between 10,000 and 25,000 yr) slightly more negative than the maximum values after the initial perturbation started (at 5000 yr) and rapidly returns to approximately the original (more positive) $\delta^{13}C$ values when the CH_4 flux is terminated. The response in $\delta^{13}C_{ocean}$ associated with the negative excursion in $\delta^{13}C_{atm}$ via the continental-weathering feedback river-flux to the ocean is much smaller (<−2‰). A relatively small amount of CH_4 released directly into the atmosphere is therefore required to provide rapid negative $\delta^{13}C$ excursions in $\delta^{13}C_{atm}$, but this cannot explain the synchronous large excursion in marine carbonates of around −5‰. The changes in $\delta^{13}C$ will be modulated by system responses to increased CO_2 levels, such as increased biomass production and/or continental weathering rates. Increased biomass production, for example, will restore $\delta^{13}C_{atm}$ to more positive values, which will in turn require larger CH_4 fluxes to provide the negative $\delta^{13}C_{atm}$ excursions in preserved terrestrial organic matter. If about 5% of CH_4 released directly into the oceans is diverted into the atmosphere, then a 10,000-yr pulse of about 25%–50% of the present global clathrate reservoir can account for the magnitude of both terrestrial and marine excursions observed across the P-T boundary (fig. 5*A*, *b*). Such a scenario would increase atmospheric CO_2 levels by about 30% and cause general global warming. The CH_4 is not very soluble in seawater and will probably be rapidly oxidized (to CO_2) in the oceans, resulting in general oceanic anoxia. This is consistent with stratigraphic observations (Erwin 1993; Knoll et al. 1996; Hallam and Wignall 1997; Isozaki 1997).

The multiple negative carbon isotope spikes we have documented are probably best explained, therefore, by episodic, punctuated release of methane from clathrates sources during progressive warming and rifting of the Tethyan passive continental margin of Gondwana (fig. 5*B*), while more gradual release of CH_4 may have preceded the sudden events well before the P-T boundary, as recorded by the steady enrichment of ^{12}C in the stratigraphic sections (fig. 5*C*). Previously it had been suggested that this sustained decrease of $\delta^{13}C_{org}$ may have been linked to orogenic expulsion of gas/oil (~−25‰) from the foreland basins flanking the active Pacific margin of Gondwana and/or contemporaneous oxidation of coal/peat (~−25‰) during relative uplift of the interior basins of Gondwana (Faure et al. 1995; Hallam and Wignall 1997). This latter model specifically addressed the onset of the well-documented global coal-hiatus in the Upper Permian–Lower Triassic (Veevers et al. 1994; Faure et al. 1995; Retallack et al. 1996) and is consistent with the postulated rapid decrease in Permo-Triassic atmospheric O_2 (Berner et al. 2000). Increasing oxidation of terrestrial peat/coal by some 30% fails to account for the magnitude of the observed negative excursions (fig. 5*D*). However, such massive oxidation would have resulted in very high atmospheric CO_2 levels, which would have had to have been removed by increased continental weathering, as opposed to increased C3 biomass production. An increase in global continental silicate weathering toward the earliest Triassic is supported by increased $^{87}Sr/^{86}Sr$ in the marine environments (Veizer et al. 1999) and changes in continental sediment yield in the Karoo basin (Ward et al. 2000). This limits the coal oxidation processes to a subsidiary role in producing the negative excursions across the P-T boundary.

No simple explanation can be provided for the presence of the positive spikes in the earliest Triassic terrestrial sections. These reversals follow the large negative excursions and negative perturbations that reverberate well into the Triassic (fig. 3). Our examples are best preserved in the Indian sections, so we cannot exclude local causes. However, we note that similar patterns occur in the Triassic marine sections (Baud et al. 1989; Margaritz et al. 1992; Jin et al. 2000), albeit at much reduced amplitudes. One possible explanation for positive changes in terrestrial $\delta^{13}C_{org}$ may be related to changes in photosynthetic processes of Gondwana plants. Present-day C4 photosynthesis occurs at low atmospheric CO_2 concentration and low water (dry) and light conditions. The average δC_{org} values of C4 plants range between −18‰ and −15‰, close to the maximum values of our positive $\delta^{13}C_{org}$ spikes in the Lower Triassic. An abrupt change of C3- to C4-dominated environments in the Miocene has resulted in a similar positive $\delta^{13}C$ spike (Cerling et al. 1993, 1997). It has been suggested that some plants may have independently evolved C4 pathways earlier that were subsequently lost (Cerling et al. 1997). Drier condition throughout the early Triassic may have favored the appearance of C4 plants or CAM-type photosynthesis in the early Triassic. No palynological data exist to refute or support such abrupt changes in photosynthetic

pathways of P-T plants. However, since the threshold for C4 plant evolution is below 500 ppmv (Ehleringer et al. 1991; Cowling 1999), it is important to first evaluate if low atmospheric P_{CO_2} values were prevalent during the early Triassic. Indeed, as discussed below, all indications are that CO_2 levels were well above present-day levels (Ekart et al. 1999).

The coincidence between the rapid eruption of the Siberian flood basalts ($> 2.0 \times 10^6$ km^3; Arthur 2000) and the severe end-Permian extinctions has been noted by many workers (Erwin 1993; Renne et al. 1995; Kamo et al. 1996; Hallam and Wignall 1997; Bowring et al. 1998). Similarly, the slightly earlier outpourings of the Emeishan flood basalts ($0.25–0.5 \times 10^6$ km^3; Thompson et al. 2001) have been implicated (Chung and Jahn 1995). Some workers have suggested that there is merit, therefore, in treating gas emissions related to these flood basalts as a source for the decrease in the carbon isotope content of marine carbonates and organics across the P-T boundary. An inordinate mass of mantle CO_2 ($\delta^{13}C \sim -6‰$) would be needed, however, to shift the $\delta^{13}C$ of marine systems to the values observed (Erwin 1993; Kump and Arthur 1997; Arthur 2000). Our modeling supports the intuition that such a source alone could not account for the large decrease in the carbon $\delta^{13}C$ of terrestrial organic materials as reported here (fig. 5*F*). However, positive spikes in $\delta^{13}C_{atm}$ may be indirectly related to the increase in atmospheric CO_2 from volcanism through increased C3 biomass production (and therefore burial). This is consistent with the results of P_{CO_2} paleobarometers on pedogenic carbonates (Ekart et al. 1999). A reasonable flux of mantle CO_2 sustained for 10,000 yr would double the terrestrial CO_2 concentrations within a further 10,000 yr. At this point increased terrestrial C3 biomass production (burial) would produce a sharp and large, positive excursion in $\delta^{13}C_{atm}$ similar to that observed in our data. This increase in CO_2 does not favor a model that involved the establishment of C4 plants since the latter thrive at relatively low atmospheric CO_2 conditions. Indeed, recent modeling indicates that the global land area favoring C4 plants (predominantly grasses) could be completely eliminated following a doubling of atmospheric CO_2 (Gillon and Yakir 2001).

Summary and Conclusions

We note an important distinction between (*a*) the gradual negative trend in $\delta^{13}C_{atm}$ and $\delta^{13}C_{ocean}$ from ~270 Ma to latest Permian and (*b*) the rapid and large negative excursions around the P-T boundary. Our modeling efforts focus on *b* and show CH_4 events to be a feasible mechanism to explain these rapid changes. They also show that episodic release of CH_4 will produce a more gradual drop, and this may have contributed to the longer-term trend preceding the P-T. However, this does not rule out other causes for the more gradual negative trends (such as faster orogenic expulsion of oil/gas, oxidation of peat, etc.). A combination of the latter processes to explain longer trends might be favored because of the huge reservoirs of light CO_2 that can be tapped over very long periods of time. Thus, although these processes cannot explain the rapid/large isotope excursions across the P-T boundary, they probably played an important role in creating the preceding gradual negative shift. In fact, we speculate that these processes probably provided the CO_2 and warmth needed to end the Paleozoic glacial era and that the combination of increased CO_2/lower O_2 played a very important (if not vital) role in the gradual ecosystem decline and minor extinctions that preceded the actual P-T event. The coincidence with the breakup of Pangea may have produced huge additional CO_2 fluxes (e.g., metamorphic) not yet included in any current models of CO_2 change.

We postulate, therefore, that a complex chain of feedback mechanisms, initially catalyzed through the rapid movement of Gondwana's continental shelf into lower latitudes, together with the disintegration of this northern marine platform in the Late Permian, can satisfactorily account for destabilization of postulated clathrates along the margins of southern Tethys and, in turn, account for the chemical stratigraphy observed during the transition from the Paleozoic to the Mesozoic.

Relatively gradual and "terminal" spiked extinctions observed across this boundary may be sought in complex nonlinear behavior of the coupled atmosphere-ocean-biosphere system throughout this time. The patterns we have observed may reflect abrupt (catastrophic) response of ecosystems to gradual forcing and thresholds (cf. Noy-Meir 1975; May 1977; Scheffer et al. 2001), such as has been inferred to explain sudden switching between bistable or multiple equilibrium states in terrestrial lakes (Scheffer et al. 1993) and ocean basins (Stomell 1961; Broecker 1997; Paillard 1998; Ganopolsiki and Rahmstorf 2001). While the carbon isotope stratigraphy across the P-T boundary cannot yet resolve details of complex feedback, we note that distinct biodiversity changes during biosphere "crises" occurred both below and

above the P-T boundary (Erwin 1993, 1994; Hallam and Wignall 1997; Looy et al. 1999; Retallack 1999; Yin et al. 2000). This suggests that rates of extinctions and recoveries may have varied in tandem and that simple single-stage extinction and recovery models, or indeed general equilibrium models (Erwin 2000; Kirchner and Weil 2000) for the most profound crises of the Phanerozoic biosphere, may not be appropriate. The longer but more gradual change preceding the negative excursion at the P-T transition may have been more important in compounding environmental stress factors that made the system susceptible to eventual dramatic collapse. The CH_4 events may, therefore, have triggered the final collapse of already stressed ecosystems, but it is important to note that the trends preceding it are also important, perhaps more so.

ACKNOWLEDGMENTS

This work was funded through grants from the South African National Research Foundation to M. J. de Wit. We thank Vijaya, Neerja Jha, Ram-Awatar, K. L. Meena, and A. P. Bhattacharyya of the Birbal Sahni Institute of Paleobotany for providing palynologically dated material; P. Ward for sharing his Karoo nodules and K. MacLeod, his isotope knowledge; J. Lee-Thorpe, J. Lanham, I. Newton, and E. Stout for help in the isotope lab; and C. Scotese and A. Smith for providing their Paleomap and Atlas software, respectively, to generate figure 1. M. Menning kindly provided a preprint of his new Permian timescale. S. Bowring was a solid sounding board throughout the study and critically reviewed a near-final version of this manuscript; thoughtful comments by L. Kump and an anonymous reviewer improved this yet further.

REFERENCES CITED

Alexander, J. 1999. Organic carbon isotope stratigraphy of the type terrestrial Karoo sequence near Laingsburg. Honors thesis, University of Cape Town.

Anderson, J. M.; Anderson, H. M.; Archangelsky, S.; Bamford, M.; Chandra, S.; Dettman, M.; Hill, R.; Mcloughlin, S.; and Rösler, O. 1999. Patterns of Gondwana plant colonisation and diversification. J. Afr. Earth Sci. 28:145–168.

Arthur, M. A. 2000. Volcanic contributions to the carbon and sulfur geochemical cycles and global change. *In* Sigurdson, H., et al., eds. Encyclopedia of Volcanoes. Academic Press, San Diego, Calif., p. 1045–1056.

Ballard, M. M.; van der Voo, R.; Hälbich, I. W. 1986. Remagnetisation in Late Permian and Early Triassic rocks from southern Africa and their implications for Pangea reconstructions. Earth Planet. Sci. Lett. 79: 412–418.

Baud, A.; Magaritz, M.; and Holser, W. T. 1989. Permian-Triassic of the Tethys: carbon isotope studies. Geol. Rundsch. 78:649–677.

Beauchamp, B. 1994. Permian climate cooling in the Canadian Arctic. *In* Klein, G. D., ed. Pangea: paleoclimate, tectonics and sedimentation during accretion: zenith and breakup of a supercontinent. Geol. Soc. Am. Spec. Pap. 288:229–246.

Becker, L.; Poreda, R. J.; Junt, A. G.; Bunch, T. E.; and Rampino, M. 2001. Impact event at the Permian-Triassic Boundary: evidence from extra-terrestrial noble gasses in fullerenes. Science 291:1530–1533.

Berner, R. A. 1994. GEOCARB II: a revised model for atmospheric CO_2 over Phanerozoic time. Am. J. Sci. 294:56–91.

Berner, R. A.; Petsh, S. T.; Lake, J. A.; Beerling, D. J.; Popp, B. N.; Lane, R. S.; Laws, E. A., et al. 2000. Isotopic fractionation and atmospheric oxygen: implications for Phanerozoic O_2 evolution. Science 287: 1630–1633.

Bowring, S. A.; Erwin, D. H.; Jin, Y. G.; Martin, M. W.; Davidek, K.; and Wang, W. 1998. U/Pb zircon geochronology and tempo of the end-Permian mass extinction. Science 280:1039–1045.

Broecker, W. 1997. Will our ride into the greenhouse future be a smooth one? GSA Today 7:1–7.

Cerling, T. E.; Harris, J. M.; MacFadden, B. J.; Leakey, M. G.; Quade, J.; Eisenmann, V.; and Ehleringer, J. R. 1997. Global vegetation change through the Miocene/Pliocene boundary. Nature 389:153–158.

Cerling, T. E.; Wang, Y.; and Quade, J. 1993. Expansion of C4 ecosystems as an indicator of global ecological change in the Late Miocene. Nature 361:344–345.

Chung, S. L., and Jahn, B. M. 1995. Plume-lithosphere interaction in generation of the Emeishan flood basalts at the Permian-Triassic boundary. Geology 23: 889–892.

Cowling, S. A. 1999. Plants and temperature: CO_2 uncoupling. Science 285:1500–1501.

DeNiro, M. J., and Hastof, C. A. 1984. Alteration of $^{15}N/^{14}N$ and $^{13}C/^{12}C$ ratios of plant matter during the initial stages of diagenesis: studies utilising archaeological specimens from Peru. Geochim. Cosmochim. Acta 49: 97–115.

Dickens, G. R.; O'Neil, J. R.; Dea, D. K.; and Oma, R. M. 1995. Dissociation of oceanic methane hydrate as a cause of the carbon isotope excursion at the end of the Paleocene. Paleoceanography 10:965–971.

Dickens, J. M. 1992. Permo-Triassic orogenic, paleoclimate and eustatic events and their implications for biotic alteration. *In* Sweet, W. C.; Zunyi, Y.; Dickens,

J. M.; and Hongfu, Y., eds. Permo-Triassic events in the eastern Tethys: stratigraphy, classification and relations with the western Tethys. Cambridge, Cambridge University Press, p. 169–174.

Edmond, J. M. 1992. Himalayan tectonics, weathering processes and the strontium isotope record in marine limestones. Science 258:1594–1597.

Egle, S. 1996. Paleo-hydrology of the Cape Fold Belt and the Karoo Basin, South Africa. Ph.D. dissertation, University of Vienna.

Egle, S.; de Wit, M. J.; and Hoernes, S. 1998. Gondwana fluids and subsurface paleo-hydrology of the Cape Fold Belt and the Karoo Basin, South Africa. J. Afr. Earth Sci. 27:63–64.

Ekart, D. D.; Cerling, T. E.; Montañex, T.-P.; and Tabor, N. J. 1999. A 400 million year carbon isotope record of pedogenic carbonate: implications for paleo-atmospheric carbon dioxide. Am. J. Sci. 299:805–927.

Erhlinger, J. R.; Sage, R. F.; Flanagan, L. B.; and Peracy, R. W. 1991. Climate change and the evolution of C4 photosynthesis. Trends Ecol. Evol. 6:95–99.

Erwin, D. H. 1993. The great Paleozoic crisis. New York, Columbia University Press.

———. 1994. The Permo-Triassic extinction. Nature 367: 231–236.

———. 2000. Life's downs and ups. Nature 404:129–130.

Eshet, Y.; Rampino, M. R.; and Visscher, H. 1995. Fungal event and palynological record of ecological crisis and recovery across the Permian-Triassic boundary. Geology 23:967–970.

Faure, K., and Cole, D. 1999. Geochemical evidence for lacustrine microbial blooms in the vast Permian main Karoo, Paraná, Falkland Islands and Huab basins of southwestern Gondwana. Palaeogeog. Palaeoclimatol. Palaeoecol. 152:189–213.

Faure, K.; de Wit, M. J.; and Willis, J. P. 1995. Late Permian global coal hiatus linked to ^{13}C-depleted CO_2 flux into the atmosphere during the final consolidation of Pangea. Geology 23:507–510.

Forster, C. B.; Logan, A.; and Summons, R. E. 1999. The Permian-Triassic boundary in Australia—oroganic carbon isotope anomalies relate to organic facies, not a biogeochemical "event." Ninth Annual V. M. Goldschmidt Conference, Houston, Lunar and Planetary Inst. Contribution 971, p. 87–88.

Ganopolsiki, A., and Rahmstorf, S. 2001. Rapid changes of glacial climate simulated in a coupled climate model. Nature 409:153–158.

Ghosh, J. G. 1999. U/Pb geochronology and structural geology across major shear zones of the southern granulite terrain of India, and $\delta^{13}C_{org}$ stratigraphy of the Gondwana coals basins of India. Ph.D. dissertation, University of Cape Town.

Gillon, J., and Yakir, D. 2001. Influence of carbonic anhydrase activity in terrestrial vegetation on the ^{18}O content of atmospheric CO_2. Science 291:2584–2587.

Goubin, N. 1976. Description et répartition des principaus pollenites Permiens, Triasiques et Jurassiques des sandages du bassin de Morondava (Madagascar). Rev. Inst. Fr. Pétrol. 20:1415–1461.

Graham, J. B.; Dudley, R.; Aguilar, N. M.; and Gans, C. 1995. Implications of the late Paleozoic oxygen pulse for physiology and evolution. Nature 375:117–120.

Gröcke, D. R.; Hesselbo, S. P.; and Jenkyns, H. C. 1999. Carbon-isotope composition of Lower Cretaceous fossil wood: ocean-atmosphere chemistry and relation to sea-level change. Geology 27:155–158.

Hälbich, I. W.; Fitch, F. J.; and Miller, J. A. 1983. Dating the Cape orogeny. Spec. Publ. Geol. Soc. S. Afr. 12: 149–164.

Hallam, A. 1992. Phanerozoic sea-level changes. New York, Columbia University Press, 266 p.

———. 1998. Interpreting sea-level. *In* Doyle, P., and Bennett, M. R., eds. Unlocking the stratigraphical record. New York, Wiley, p. 421–439.

Hallam, A., and Wignall, P. B. 1997. Mass extinctions and their aftermath. New York, Oxford University Press.

Hesselbo, F. P.; Gröke, D. R.; Jenkyns, H. C.; Bjerrum, C. J.; Farrimond, P.; Morgans Bell, H. S.; and Green, O. R. 2000. Massive dissociation of gas hydrate during a Jurassic oceanic anoxic event. Nature 406:392–395.

Hottinski, R. M.; Bice, K. L.; Kump, L. R.; Najjar, R. G.; and Arthur, M. A. 2001. Ocean stagnation and end-Permian anoxia. Geology 29:7–10.

Isozaki, Y. 1997. Permo-Triassic boundary superanoxia and stratified superocean: records from lost deep sea. Science 276:235–238.

Jin, Y. G.; Wang, Y.; Wang., W.; Shang, Q. H.; Cao, C. Q.; and Erwin, D. H. 2000. Pattern of marine mass extinction near the P-T boundary in South China. Science 289:432–436.

Kajiwara, T.; Yamakita, S.; Ishida, K.; Ishiga, H.; and Imai, A. 1994. Development of large anoxic stratified ocean and its temporary massive mixing at the Permian/Triassic boundary supported by sulfur isotope record. Palaeogeogr. Palaeoclimatol. Palaeoecol. 111:367–379.

Kamo, S. L.; Czamanske, G. K.; and Krogh, T. E. 1996. A minimum of U/Pb age for Siberian flood volcanism. Geochim. Cosmochim. Acta 60:3505–3511.

Kennett, J. P.; Cannariato, K. G.; Hendy, I. L.; and Behl, R. J. 2000. Carbon isotopic evidence for methane hydrate instability during quaternary interstadials. Science 288:128–133.

Kirchner, J. W., and Weil, A. 2000. Delayed biological recovery from extinctions throughout the fossil record. Nature 404:177–180.

Knoll, A. H.; Bambach, R. K.; Canfield, D. E.; and Grotzinger, J. P. 1996. Comparative earth history and Late Permian mass extinction. Science 273:452–457.

Krull, E. S., and Retallack, G. J. 2000. δ^{13}C depth profiles from paleosols across the Permian-Triassic boundary: evidence for methane release. Geol. Soc. Am. Bull. 112:1459–1472.

Krull, E. S.; Retallack, G. J.; Campbell, H. J.; and Lyon, G. L. 2000. $\delta^{13}C_{org}$ chemostratigraphy of the Permian-Triassic boundary in the Maitai Group, New Zealand: evidence for high-latitudinal methane release. N. Z. J. Geol. Geophys. 43:21–32.

Kump, L. R., and Arthur, M. A. 1997. Global chemical

erosion during the Cenozoic: weatherability balances the budget. *In* Ruddiman, W., ed. Tectonics uplift and climate change. New York, Plenum, p. 399–426.
Kvenvolden, K. A. 1988. Methane hydrates and global climate. Global Biogeochem. Cycles 2:221–229.
———. 1993. Gas hydrates: geological perspective and global change. Rev. Geophys. 31:173–187.
Looy, C. V. 2000. The Permian-Triassic biotic crisis: collapse and recovery of terrestrial ecosystems. Ph.D. dissertation, University of Utrecht.
Looy, C. V.; Burgman, W. A.; Dilcher, D. L; and Visscher, H. 1999. The delayed resurgence of equatorial forests after the Permian-Triassic ecological crisis. Proc. Natl. Acad. Sci. U.S.A. 96:13,857–13,862.
MacLeod, K. G.; Smith, R. M. H.; Koch, P. L.; and Ward, D. P. 2000. Timing of mammal-like reptile extinction across the Permian-Triassic boundary in South Africa. Geology 28:227–230.
Margaritz, M.; Krishnamurthy, R. V.; and Holser, W. T. 1992. Parallel trends in organic and inorganic carbon isotopes across the Permian-Triassic boundary. Am. J. Sci. 292:727–739.
Max, M. D. 2000. Natural gas hydrate in oceanic and permafrost environments. Dordrecht, Kluwer.
May, R. M. 1977. Thresholds and break points in ecosystems with a multiplicity of stable states. Nature 269:471–477.
Menning, M. 2001. A Permian time scale 2000 and correlation of marine and continental sequences using Illawara reversal (265 Ma). Natura Bresciana Ann. Mus. Civ. Sci. Nat. Monogr. 25:355–362.
Metcalfe, I.; Nicol, R. S.; Black, L. P.; Mundil, R.; Renne, P.; Jagodzinski, E. A.; and Wang, C. 1999. Isotope geochronology of the Permian-Triassic boundary and mass extinction in South China. *In* Yin, H., and Tong, J., eds. Pangea and the Paleozoic-Mesozoic transition. Wuhan, China University of Geoscience Press.
Morante, R. 1996. Permian and early Triassic isotopic records of carbon and strontium in Australia and a scenario of events about the Permian-Triassic boundary. Historical Biology 11:289–310.
Noy-Meir, I. 1975. Stability of grazing systems: an application of predators-prey graphs. J. Ecol. 63:459–481.
Oberhänsli, H.; Hsü, K. J.; Piasecki, S.; and Weissert, H. 1989. Permian-Triassic carbon isotope anomaly in Greenland and the Southern Alps. Historical Biology 2:37–49.
Opdyke, N. D.; Mashayandebun, M.; and de Wit, M. J. 2001. A new paleomagnetic pole for the Dwyka System and correlative sediments in subsaharan Africa. J. Afr. Earth Sci. 33:143–154.
Padden, M.; Weissert, H.; and de Rafelis, M. 2001. Evidence for Late Jurassic release of methane from gas hydrate. Geology 29:193–288.
Paillard, D. 1998. The timing of Pleistocene glaciations from a simple multiple-state climate model. Nature 391:378–381.
Plumstead, E. P. 1969. Three thousand million years of plant life in Africa. Geol. Soc. S. Afr. 76:1–72.
Rakotosolofo, N. 1999. Geology, carbon isotope stratigraphy and paleomagnetism of the Karoo sequences of the southern Morondara basin, SW Madagascar. M.S. thesis, Rand Afrikaans University, Johannesburg.
Renne, P. R.; Zichao, Z.; Richards, M. A.; Black, M. T.; and Basu, A. R. 1995. Synchrony and causal relations between Permian-Triassic boundary crises and Siberian flood volcanism. Science 269:1413–1416.
Retallack, G. J. 1995. Permian-Triassic life crisis on land. Science 267:77–80.
———. 1999. Postapocalyptic greenhouse paleoclimate revealed by earliest Triassic paleosols in the Sydney basin, Australia. Geol. Soc. Am. Bull. 111:52–70.
Retallack, G. J.; Veevers, J. J.; and Morante, R. 1996. Global coal gap between Permian-Triassic extinction and Middle Triassic recovery of peat-forming plants. Geol. Soc. Am. Bull. 108:195–207.
Rubidge, B. S. 1995. Biostratigraphy of the Beaufort Group (Karoo supergroup). Geol. Surv. S. Afr. Biostratigr. Ser. 1, 46 p.
Scheffer, M.; Carpenter, S.; Foley, J. A.; Folke, G.; and Walker, B. 2001. Catastrophic shifts in ecosystems. Nature 413:591–596.
Scheffer, M.; Hosper, S. M.; Meijer, M.-L.; Moss, B.; and Jeppesen, E. 1993. Alternative equilibria in shallow lakes. Tree 8:275–279.
Schlesser, G. H. 1992. $\delta^{13}C$ pattern in a forest tree as an indicator of carbon transfer in trees. Ecology 73: 1922–1935.
Scotese, C. R. 2000. Atlas of earth history. Vol. 1. Paleogeography Paleomap Project, University of Texas, Arlington. http://www.scotese.com.
Scotese, C. R.; Boucout, A. J.; and McKerrow, W. S. 1999. Gondwana paleogeography and paleo-climatology. J. Afr. Earth Sci. 28:99–114.
Singh, V., and Tiwari, R. S. 1982. Pattern of miofloras through Permo-Triassic transition in borehole RAD-2, East Raniganj Coalfield, West Bengal. Geophytology 12:181–186.
Smith, A. G. 1999. Gondwana: its shape, size and position from Cambrian to Triassic times. J. Afr. Earth Sci. 28:71–98.
Smith, B. N.; Oliver, J.; and McMillan, C. 1976. Influence of carbon source, oxygen concentration, light intensity and temperature on $^{13}C/^{12}C$ ratios in plant tissues. Bot. Gaz. 137:99–104.
Srivastava, S. C., and Bhattacharyya, A. P. 1996. Permian-Triassic palynofloral succession in subsurface from Bazargaon, Nagpur District, Maharashtra. Palaeobotanist 43:10–15.
Srivastava, S. C., and Jha, N. 1990. Permian-Triassic palynofloral transition in Godavari Graben, Andhra Pradesh. Palaeobotanist 38:92–97.
———. 1995. Palynostratigraphy and correlations of Permian-Triassic sediments in Budharam Area, Godavari Graben, India. J. Geol. Soc. India 46:647–653.
Stanley, S. M., and Yang, X. 1994. A double mass extinction at the end of the Paleozoic era. Science 266: 1340–1344.
Stommel, H. M. 1961. Thermohaline convection with two stable regimes of flow. Tellus 13:224–230.

Thackeray, J. F.; van der Merwe, N. J.; Lee-Thorpe, J. A.; Sillen, A.; Lanham, J. L.; Smith, R.; Keyser, A.; and Monteiro, P. M. F. 1990. Carbon isotope evidence for Late Permian therapsids teeth, for a progressive change in atmospheric CO_2 composition. Nature 347: 751–753.

Thompson, G. M.; Jason, R. A.; Song, X.; and Jolley, D. W. 2001. Emeishan basalts, SW China reappraisal of the formation's type area stratigraphy and a discussion of its significance as a large igneous province. J. Geol. Soc. Lond. 158:593–599.

Tieszen, L. J. 1991. Natural variation in the carbon isotope values of plants: implications for archaeology, ecology, and paleontology. J. Archaeol. Sci. 181: 227–248.

Tiwari, R. S. 1996. Palynoevents stratigraphy in Gondwana sequence of India. Gondwana IX, Conference Proceedings, vol. 1. Geol. Soc. India, Oxford, p. 3–19.

Tiwari, R. S., and Ram-Awatar. 1987. Palynostratigraphic studies of sub-surface Supra-Barakar sediments from Korar Coalfield, Son Valley, Madhya Pradesh. Geophytology 17:256–264.

Tiwari, R. S., and Singh, V. 1983. Miofloral transition at Raniganj-Panchet boundary in East Raniganj Coalfield and its implication on P-T time boundary. Geophytology 13:227–234.

———. 1986. Palynological evidence for P-T boundary in Raniganj Coalfield, Damodar Basin, India. Bull. Geol. Mining Metallurg. Soc. India 54:256–264.

Tiwari, R. S., and Tripathi, A. 1988. Palynological zones and their climatic inference in the coal-bearing Gondwana of peninsular India. Palaeobotanist 36:87–101.

———. 1992. Marker assemblage-zones of spores and pollen species through Gondwana Palaeozoic and Mesozoic sequence in India. Palaeobotanist 40:194–236.

Tiwari, R. S.; Vijaya; and Meena, K. L. 1992. Palynological sequence and relationship of subsurface Permian-Triassic sediments in eastern Raniganj Coalfield, West Bengal, India. Geophytology 21:21–32.

Trouw, R. A. J., and de Wit, M. J. 1999. Relation between Gondwanide orogen and contemporaneous intra-cratonic deformation. J. Afr. Earth Sci. 28:203–214.

Turner, B. R. 1999. Tectonostratigraphical development of the upper Karoo foreland basin: orogenic unloading versus thermally induced Gondwana rifting. J. Afr. Earth Sci. 28:215–234.

Twitchett, R. J.; Looy, C. V.; Morante, R.; Visscher, H.; and Wignall, P. B. 2001. Rapid and near-synchronous collapse of marine and terrestrial ecosystems during the end Permian biotic crisis. Geology 29:351–354.

van der Merwe, N. J., and Medina, E. 1991. The canopy effect, carbon isotope ratios and foodwebs in Amazonia. J. Archaeol. Sci. 18:249–259.

Veevers, J. J.; Conagha, P. J.; and Shaw, S. E. 1994. Turning point in Pangean environmental history at the Permian/Triassic (P-Tr) boundary: paleoclimate, tectonics and sedimentation during accretion, zenith and break-up of a supercontinent. *In* Klein, G. D., ed. Geol. Soc. Am. Spec. Pap. 228:187–196.

Veizer, J.; Ala, D.; Azmy, K.; Bruckshen, P.; Buhl, D.; Bruhn, F.; Carden, G. A. F.; and Diener, A. 1999. $^{87}Sr/^{86}Sr$, $\delta^{13}C$ and $\delta^{18}O$ evolution of Phanerozoic seawater. Chem. Geol. 161:59–88.

Vijaya and Tiwari, R. S. 1982. Pattern of miofloras through P-T transition in bore-hole RAD-2, East Raniganj Coalfield, W. Bengal. Geophytology 12:181–186.

———. 1986. Role of spore-pollen species in demarcating the P-T boundary in Raniganj Coalfield, West Bengal. Palaeobotanist 35:242–248.

Visscher, H.; Brinkhuis, H.; Dilcher, D. L.; Elsik, W. C.; Eshet, Y.; Looy, C. V.; Rampino, M. R.; and Traverse, A. 1996. The terminal Paleozoic fungal event: evidence of terrestrial ecosystem destabilisation and collapse. Proc. Natl. Acad. Sci. 93:2155–2158.

Ward, P. D.; Montgomery, D. R.; and Smith, R. 2000. Altered river morphology in South Africa related to the Permian-Triassic extinction. Science 289: 1740–1743.

White, J. W.; Cials, P.; Figge, R. A.; Kenny, R.; and Markgraf, V. 1994. A high resolution record of atmospheric CO_2 content from carbon isotopes in peat. Nature 367: 153–156.

Wright, R. P., and Askin, R. A. 1987. The Permian-Triassic boundary in the southern Morondava basin of Madagascar as defined by plant microfossils. Am. Geophys. Union Monogr. 39:157–166.

Xu, D.-Y., and Yan, Z. 1993. Carbon isotope and iridium event markers near the Permian/Triassic boundary in the Meishan section, Zhejiang Province, China. Paleogeogr. Paleoclimatol. Paleoecol. 104:171–176.

Yin, H.; Sweet, W. C.; Glenister, B. F.; Kotlyar, G.; Kozur, H.; Newell, N. D.; Sheng, J. Y.; and Zakharov, Y. D. 1996. Recommendations of the Meishan section as global stratotype section and point for basal boundary of Triassic system. Newsl. Strat. 34:81–108.

Zhang, R.; Follows, M. J.; Grotzinger, J. P.; and Marshal, J. 2001. Could the Late Permian deep ocean have been anoxic? Paleoceanography 16:317–329.